PUBLISHED IN APJL, 800, L14
Preprint typeset using LaTeX style emulateapj v. 5/2/11

arXiv:1410.5325v2 [astro-ph.EP] 10 Mar 2015

ETHYL CYANIDE ON TITAN: SPECTROSCOPIC DETECTION AND MAPPING USING ALMA

M. A. CORDINER[1,2], M. Y. PALMER[1,3], C. A. NIXON[1], P. G. J. IRWIN[4], N. A. TEANBY[5], S. B. CHARNLEY[1], M. J. MUMMA[1], Z. KISIEL[6], J. SERIGANO[1,2], Y.-J. KUAN[7,8], Y.-L. CHUANG[7], K.-S. WANG[8]

Published in ApJL, 800, L14

ABSTRACT

We report the first spectroscopic detection of ethyl cyanide (C_2H_5CN) in Titan's atmosphere, obtained using spectrally and spatially resolved observations of multiple emission lines with the Atacama Large Millimeter/submillimeter Array (ALMA). The presence of C_2H_5CN in Titan's ionosphere was previously inferred from Cassini ion mass spectrometry measurements of $C_2H_5CNH^+$. Here we report the detection of 27 rotational lines from C_2H_5CN (in 19 separate emission features detected at $> 3\sigma$ confidence), in the frequency range 222-241 GHz. Simultaneous detections of multiple emission lines from HC_3N, CH_3CN and CH_3CCH were also obtained. In contrast to HC_3N, CH_3CN and CH_3CCH, which peak in Titan's northern (spring) hemisphere, the emission from C_2H_5CN is found to be concentrated in the southern (autumn) hemisphere, suggesting a distinctly different chemistry for this species, consistent with a relatively short chemical lifetime for C_2H_5CN. Radiative transfer models show that C_2H_5CN is most concentrated at altitudes $\gtrsim 200$ km, suggesting production predominantly in the stratosphere and above. Vertical column densities are found to be in the range $(1\text{-}5)\times10^{14}$ cm^{-2}.

Subject headings: planets and satellites: individual (Titan) — planets and satellites: atmospheres — techniques: interferometric — techniques: imaging spectroscopy

1. INTRODUCTION

Saturn's largest moon Titan has a thick (1.45 bar) atmosphere composed primarily of molecular nitrogen (98%) and methane (approximately 2%). Remote and in-situ measurements (see the review by Bézard et al. 2014), have also revealed the presence of a diverse population of trace hydrocarbons and nitrogen-bearing compounds, the presence of which can be explained as a consequence of a complex gas-phase photochemistry, driven by photodissociation/ionization and cosmic rays (Wilson & Atreya 2004).

Multiple studies have predicted the existence of ethyl cyanide (C_2H_5CN, also known as propionitrile) on Titan, but a firm confirmation of its presence has been elusive until now. Capone et al. (1981) suggested that C_2H_5CN could be formed as a recombination product of complex nitrile ions produced in three-body association reactions in the dense, lower atmosphere. More recent photochemical models by Krasnopolsky (2009) and Loison et al. (2014) predict C_2H_5CN to be abundant throughout the atmosphere. In laboratory plasma-discharge experiments designed to simulate Titan's photochemistry, C_2H_5CN is among the most abundant molecules produced (*e.g.* Thompson et al. 1991; Coll et al. 1999; Fujii & Arai 1999), and crystalline C_2H_5CN has been suggested as an explanation for the broad emission feature at 221 cm^{-1} seen in the Voyager IRIS data (Khanna 2005). Nevertheless, previous spectroscopic studies have failed to find gas-phase ethyl cyanide; abundance upper limits have been obtained of 8×10^{-9} from the Cassini Composite Infrared Spectrometer (CIRS) and 2×10^{-9} from IRAM 30-m microwave spectroscopy (de Kok et al. 2008 and Marten et al. 2002, respectively).

The presence of C_2H_5CN was strongly implied by the detection of $C_2H_5CNH^+$ by the Cassini Ion and Neutral Mass Spectrometer (INMS) (Vuitton et al. 2007). This nitrile ion was theorized to form primarily by proton transfer from $HCNH^+$ and $C_2H_5{}^+$ to neutral C_2H_5CN. A spectroscopic detection of C_2H_5CN would provide the first conclusive proof for the presence of ethyl cyanide in Titan's atmosphere and help validate the conclusions of the INMS studies. Gas-phase synthesis of C_2H_5CN is not well understood, and the chemical models of Krasnopolsky (2009) and Loison et al. (2014) differ in their predicted abundances by 2-3 orders of magnitude. Accurate measurements of the C_2H_5CN atmospheric distribution are required in order to constrain models for the formation of nitriles and other large organic molecules, which will lead to improvements in our understanding of the complex photochemistry occurring on Titan and on other bodies with nitrogen and methane-rich atmospheres.

In this study, we employ millimeter-wave data obtained from the Atacama Large Millimeter/submillimeter Array (ALMA) Science Archive[9] to search for and map rotational emission lines from C_2H_5CN in Titan's atmosphere, and compare the spatial distribution of C_2H_5CN emission with that of other, previously-identified molecules.

2. OBSERVATIONS

Interferometric observations of Titan were made between UT 2012-07-03 23:22:14 and 2012-07-04 01:06:18 as part of

martin.cordiner@nasa.gov
[1] NASA Goddard Space Flight Center, 8800 Greenbelt Road, Greenbelt, MD 20771, USA.
[2] Department of Physics, Catholic University of America, Washington, DC 20064, USA.
[3] Department of Chemistry, St. Olaf College, 1520 St. Olaf Avenue, Northfield, MN 55057, USA.
[4] Atmospheric, Oceanic and Planetary Physics, Clarendon Laboratory, University of Oxford, Parks Road, Oxford, OX1 3PU, UK.
[5] School of Earth Sciences, University of Bristol, Wills Memorial Building, Queen's Road, Bristol, BS8 1RJ, UK.
[6] Institute of Physics, Polish Academy of Sciences, Al. Lotnikøw 32/46, 02-668 Warszawa, Poland.
[7] National Taiwan Normal University, Taipei 116, Taiwan, ROC.
[8] Institute of Astronomy and Astrophysics, Academia Sinica, Taipei 106, Taiwan, ROC.

[9] https://almascience.nrao.edu/alma-data/archive

ALMA project 2011.0.00319.S (for the purpose of flux calibration). Two 4 minute integrations were obtained using the dual-sideband Band 6 receiver, with twenty 12-m antennae in the telescope array, providing baselines in the range 21-402 m. Due to the high sensitivity of ALMA, even these short integrations permitted the detection of weak spectral lines on Titan. The correlator was configured to observe four basebands, with frequencies 221.48-223.35 GHz and 223.48-225.35 GHz in the lower sideband, and 236.48-238.36 GHz and 239.48-241.36 GHz in the upper sideband, with 3840 channels per spectral window. The channel spacing was 488 kHz which (after Hanning smoothing by the correlator), leads to a spectral resolution of 976 kHz (or 1.3 km s^{-1} at 224 GHz). Weather conditions were good, with 1.7 mm of precipitable water vapor at zenith. The bright quasar 3C 279 was observed for bandpass calibration. The telescope was configured to track Titan's ephemeris position, updating the coordinates of the phase center in real-time.

The data obtained from the ALMA Science Archive were already processed using the standard scripts and protocols provided by the Joint ALMA Observatory. This included routine flagging, bandpass calibration and complex gain calibration. The measured continuum flux density for each baseline was scaled to match the Butler-JPL-Horizons 2010 Titan flux model (see ALMA Memo #594[10]), which is expected to be accurate to within 15%. Continuum-subtraction of the visibility amplitudes was performed using the `uvcontsub` task in the NRAO CASA software (version 4.2.1) (McMullin et al. 2007), and imaging was carried out using the `clean` task. Deconvolution of the point-spread function (PSF) was performed for each spectral channel using the Hogbom algorithm, with natural visibility weighting and a threshold flux level of twice the expected RMS noise. The image pixel sizes were set to $0.1'' \times 0.1''$. The resulting spatial resolution (FWHM of the Gaussian restoring beam at 223.5 GHz) was $0.85'' \times 0.67''$ (long axis 57.3° clockwise from celestial north). This resolution element corresponds to 5860 × 4620 km at Titan's geocentric distance of 9.51 AU at the time of observation (compared with Titan's 5,150 km diameter).

The images were transformed from equatorial coordinates to (projected) linear distances with respect to the center of Titan, and the spectral coordinate scale of each image was Doppler-shifted to Titan's rest frame using the JPL Horizons Topocentric radial velocity.

3. RESULTS

The observed spectra recorded in each of the four basebands are shown in Fig. 1. These were obtained by integrating the reduced ALMA data cubes within a circular region of radius $1.1''$ from the center of Titan (7,500 km at Titan's distance). This circle enclosed the flux within $2\sigma_{PSF}$ of Titan's surface, where σ_{PSF} is the standard deviation of the major axis of the restoring beam. Negligible flux was found to lie outside of this region.

Spectral peaks were assigned using the Splatalogue database for astronomical spectroscopy[11], with frequencies obtained from the Cologne Database for Molecular Spectroscopy (Müller et al. 2001) and the JPL catalog[12]. The detected transitions are given in Table 1. The spectra are

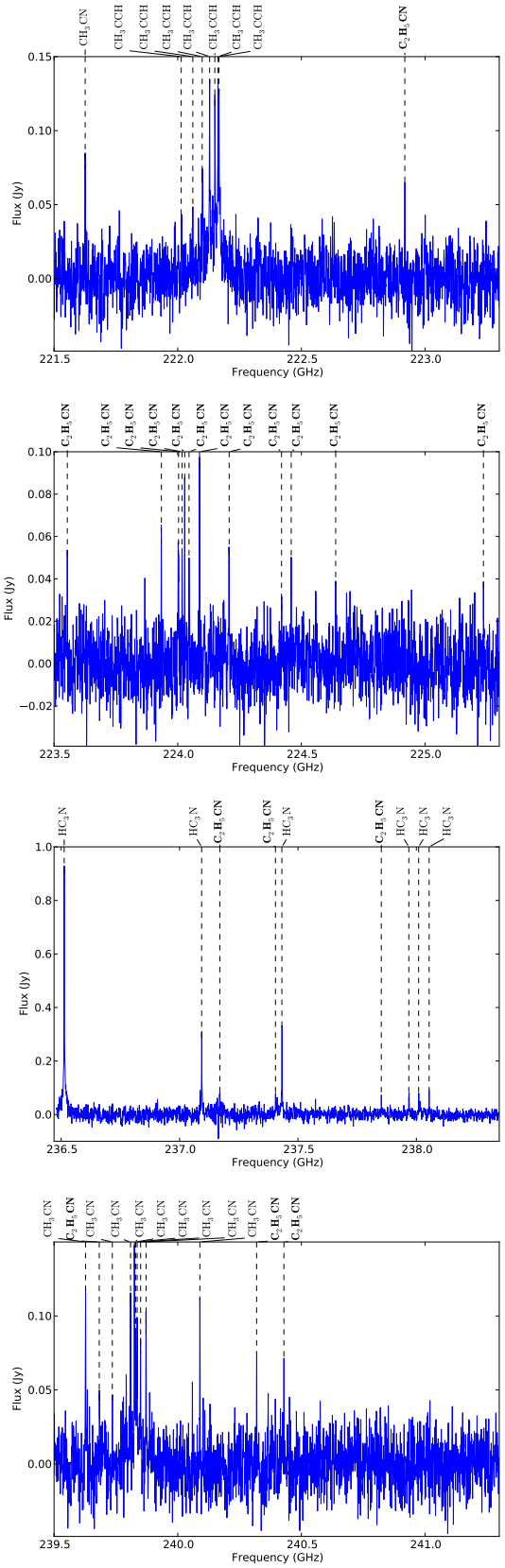

FIG. 1.— ALMA spectra observed 2012 July 3-4, integrated over a circular region of radius $1.1''$ centered on Titan. Titan's continuum emission has been subtracted. Prominent emission lines are assigned by species; bold typeface highlights the C_2H_5CN emission features. The small absorption feature at 237.146 GHz is attributed to ozone in the Earth's atmosphere.

[10] https://science.nrao.edu/facilities/alma/aboutALMA/Technology/ALMA_Memo_Series/alma594/memo594.pdf

[11] http://www.cv.nrao.edu/php/splat/

[12] http://spec.jpl.nasa.gov/

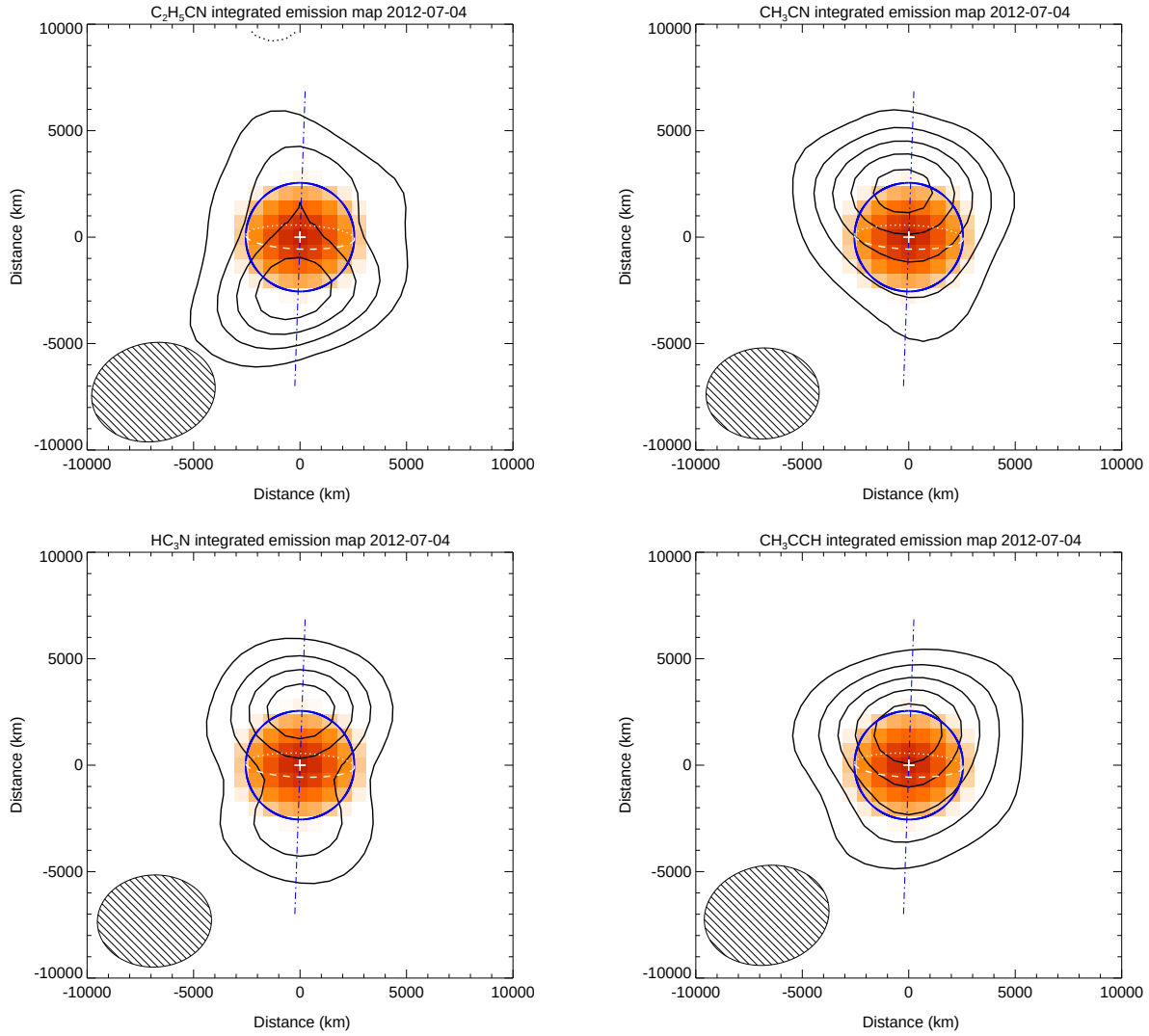

FIG. 2.— Integrated emission contour maps for C_2H_5CN, HC_3N, CH_3CN and CH_3CCH. The 221-225 GHz continuum is shown in orange. The coordinate scale is in Titan-projected distances (white cross denotes the position of the phase center). Axes are aligned in the equatorial coordinate system. Contour intervals (in units of σ — the RMS noise level of each map), are as follows: C_2H_5CN: 3σ, HC_3N: 8σ, CH_3CN: 3σ, CH_3CCH: 5σ. The blue circle represents Titan's surface (dashed white curve is the equator), and the dot-dashed blue line is the polar axis, oriented 2.0° clockwise from vertical, with the north pole tilted toward the observer by 12.7°. Titan's Earth-facing hemisphere was almost fully illuminated at the time of observation, with a (Sun-target-observer) phase angle of 5.9°. The FWHM of the Gaussian restoring beam ($0.85'' \times 0.67''$) and its orientation are shown as hatched ellipses.

sufficiently uncrowded that unambiguous assignments were possible for all detected lines. Nineteen separate C_2H_5CN rotational emission features (many of which are blends of several transitions) were detected at greater than 3σ confidence. Emission from HC_3N, vibrationally-excited CH_3CN and CH_3CCH was also detected. An additional 153 C_2H_5CN lines lie within the observed spectral range, but these were too weak to be detected individually.

Contour maps showing the spatial distributions of emission from the observed species are shown in Fig. 2, overlaid upon the 221-225 GHz continuum flux (shown in each panel as an orange bitmap). The contour maps were obtained by integrating over the strongest line(s) observed for each species. For C_2H_5CN, the strongest six lines in the range 223.9-224.1 GHz (shown in Fig. 3(b)) were summed to improve the signal-to-noise ratio of the map. For HC_3N, only the strongest ($J = 26-25$) line was used, and for CH_3CN and CH_3CCH, integration was performed over the blended multiplets at 239.8 GHz and 222.1 GHz, respectively. The peak signal-to-noise ratios of the resulting maps were as follows: C_2H_5CN: 15, HC_3N: 40, CH_3CN: 17, CH_3CCH: 29.

Adopting a similar strategy to Cordiner et al. (2014), the spatially-integrated C_2H_5CN emission lines in the range 223.9-224.2 GHz were modeled using the line-by-line radiative transfer module of the NEMESIS atmospheric retrieval code (Irwin et al. 2008). There are 13 C_2H_5CN transitions in this range (see Table 1), spanning a broad range of upper-state energies (150-300 K), and providing sufficient information on the C_2H_5CN abundance and excitation to adequately constrain our models. A lack of interloping lines from other species in this range facilitated accurate abundance retrievals. The atmospheric temperature profile was generated from a combination of Cassini CIRS and HASI measurements (Flasar et al. 2005; Fulchignoni et al. 2005), and the abundances of nitrogen and methane isotopologues and aerosols were the same as used by Teanby et al. (2013). Spectral line parameters and partition functions were taken from the JPL catalog. The Lorentzian broadening half-width at 296 K

TABLE 1
DETECTED TRANSITIONS AND UPPER-STATE ENERGIES

Species	Frequency (GHz)	Transition	E_u (K)
C_2H_5CN	222.918	$25_{1,24}$–$24_{1,23}$	142
C_2H_5CN	223.554	$26_{0,26}$–$25_{0,25}$	147
C_2H_5CN	223.934	$25_{3,23}$–$24_{3,22}$	150
C_2H_5CN	224.002	$25_{10,15}$–$24_{10,14}$	251
C_2H_5CN	224.002	$25_{10,16}$–$24_{10,15}$	251
C_2H_5CN	224.003	$25_{9,17}$–$24_{9,16}$	230
C_2H_5CN	224.003	$25_{9,16}$–$24_{9,15}$	230
C_2H_5CN	224.018	$25_{11,14}$–$24_{11,13}$	274
C_2H_5CN	224.018	$25_{11,15}$–$24_{11,14}$	274
C_2H_5CN	224.028	$25_{8,18}$–$24_{8,17}$	211
C_2H_5CN	224.028	$25_{8,17}$–$24_{8,16}$	211
C_2H_5CN	224.046	$25_{12,13}$–$24_{12,12}$	300
C_2H_5CN	224.046	$25_{12,14}$–$24_{12,13}$	300
C_2H_5CN	224.088	$25_{7,19}$–$24_{7,18}$	194
C_2H_5CN	224.088	$25_{7,18}$–$24_{7,17}$	194
C_2H_5CN	224.207	$25_{6,20}$–$24_{6,19}$	180
C_2H_5CN	224.208	$25_{6,19}$–$24_{6,18}$	180
C_2H_5CN	224.420	$25_{5,21}$–$24_{5,20}$	168
C_2H_5CN	224.459	$25_{5,20}$–$24_{5,19}$	168
C_2H_5CN	224.639	$25_{4,22}$–$24_{4,21}$	158
C_2H_5CN	225.236	$25_{4,21}$–$24_{4,20}$	158
C_2H_5CN	237.170	$26_{3,23}$–$25_{3,22}$	162
C_2H_5CN	237.405	$26_{2,24}$–$25_{2,23}$	158
C_2H_5CN	237.852	$27_{2,26}$–$26_{2,25}$	165
C_2H_5CN	239.683	$27_{1,26}$–$26_{1,25}$	165
C_2H_5CN	240.319	$28_{1,28}$–$27_{1,27}$	169
C_2H_5CN	240.429	$28_{0,28}$–$27_{0,27}$	169
HC_3N	236.513	26–25	153
HC_3N $v_7 = 1$	237.093	26–25 $1e$	474
HC_3N $v_7 = 1$	237.432	26–25 $1f$	474
HC_3N $v_7 = 2$	237.968	26–25 $0e$	792
HC_3N $v_7 = 2$	238.010	26–25 $2e$	795
HC_3N $v_7 = 2$	238.054	26–25 $2f$	795
CH_3CN $v_8 = 1$	221.626	12_1–11_{-1}	588
CH_3CN $v_8 = 1$	239.627	13_1–12_{-1}	600
CH_3CN $v_8 = 1$	239.736	13_4–12_4	773
CH_3CN $v_8 = 1$	239.808	13_2–12_2	661
CH_3CN $v_8 = 1$	239.825	13_4–12_{-4}	667
CH_3CN $v_8 = 1$	239.830	13_1–12_1	626
CH_3CN $v_8 = 1$	239.836	13_0–12_0	606
CH_3CN $v_8 = 1$	239.850	13_3–12_{-3}	630
CH_3CN $v_8 = 1$	239.872	13_2–12_{-2}	608
CH_3CN $v_8 = 1$	240.090	13_{-1}–12_1	600
CH_3CCH	222.014	13_6–12_6	334
CH_3CCH	222.061	13_5–12_5	255
CH_3CCH	222.099	13_4–12_4	190
CH_3CCH	222.129	13_3–12_3	139
CH_3CCH	222.150	13_2–12_2	103
CH_3CCH	222.163	13_1–12_1	82
CH_3CCH	222.167	13_0–12_0	75

Note. Primary spectroscopic sources for molecular line frequencies: C_2H_5CN — Brauer et al. (2009), HC_3N — Thorwirth et al. (2000), CH_3CN — Boucher et al. (1980), CH_3CCH — Dubrulle et al. (1978).

was assumed to be 0.075 cm^{-1} atm^{-1}, with a temperature-dependence exponent of 0.50.

Under the assumption that the model temperature/abundance/aerosol profiles profiles do not vary with latitude and longitude, the integrated flux per spectral channel was calculated using a 10-point trapezium-rule integration from the center of Titan's disk to the edge of the model atmosphere (at an altitude of 1000 km). Initially, least-squares

TABLE 2
BEST-FITTING C_2H_5CN MODEL ABUNDANCES AND VERTICAL COLUMN DENSITIES

Model	Abundance (ppb)	z_r[a] (km)	χ^2	N (cm^{-2})
Step (100 km)	0.79	100	1.43	1.3×10^{15}
Step (200 km)	3.24	200	1.01	4.6×10^{14}
Step (300 km)	9.25	300	0.97	1.7×10^{14}
Step (400 km)	73.1	400	0.98	2.1×10^{14}
Gradient	1.30	292	0.97	3.6×10^{14}

[a]Reference altitude for abundance.

fits to the observed spectra were performed using C_2H_5CN abundance profiles with constant mixing ratio above a specified cutoff altitude z_c and zero abundance below. In these 'step' models, z_c values in the range 100-400 km were tried, and the best-fitting abundances for each are given in Table 2. Reduced χ^2 values are also given, and the corresponding continuum-subtracted spectral models are shown in Fig. 3.

The z_c = 300 and 400 km models (green and magenta solid curves, respectively), provide a near-perfect fit to the observations, accurately reproducing the intensities, frequencies and widths of all the spectral features attributed to C_2H_5CN. The quality of these fits confirms that our C_2H_5CN line assignments are secure. As can be seen from the close-up spectral region in Fig. 3c, our models show that pressure-broadening wings begin to become significant for $z_c \lesssim 200$ km, but no clear wings are apparent above the noise level in the observed spectra, indicating that the majority of Titan's C_2H_5CN must be confined to higher altitudes. Accordingly, the z_c = 100 km model (orange dashed curve) provides a poor fit to the observations.

Due to vertical mixing, model profiles with an abrupt abundance cutoff are unlikely to represent the true C_2H_5CN profile, so the spectrum was also fitted using a more realistic two-parameter 'gradient' model, in which the abundance varies smoothly as a function of altitude. The free parameters in this model were the abundance at a reference altitude z_r = 292 km, and the slope, given as a fraction (f_H) of the atmospheric pressure scale height. Condensation of C_2H_5CN was assumed to occur at altitudes $\lesssim 100$ km based on the saturated vapor pressure curve of Lide & Kehiaian (1994). The best-fitting abundance at z_r was found to be 1.3 ± 0.4 ppb, with a retrieved fractional scale height of $f_H = 4.6 \pm 1.1$. Despite slightly stronger line wings, this model (blue solid curve) also matches the observations extremely well.

Vertical column densities (N) for the four models are given in Table 2. The models that fit the data well have values in the range $(1-5) \times 10^{14}$ cm^{-2}.

4. DISCUSSION

4.1. *C_2H_5CN Vertical Mixing Ratio Profile*

Confirmation of the presence of ethyl cyanide in Titan's atmosphere provides an important test and validation of the Cassini INMS result. Although a near-perfect fit to our observed ALMA spectrum was obtained using a step model for the C_2H_5CN VMR profile (with cutoff altitude at 300 km), a smoothly-varying profile is expected to be more realistic. The shape of the retrieved 'gradient' profile (shown by the solid blue curve in Fig. 3a) is constrained primarily by the requirement of a low abundance at $z \lesssim 200$ km, and is largely unconstrained at altitudes above about 600 km, where the atmospheric density is low. Similar to the case of HNC (Moreno et al. 2012; Cordiner et al. 2014), the steep vertical abun-

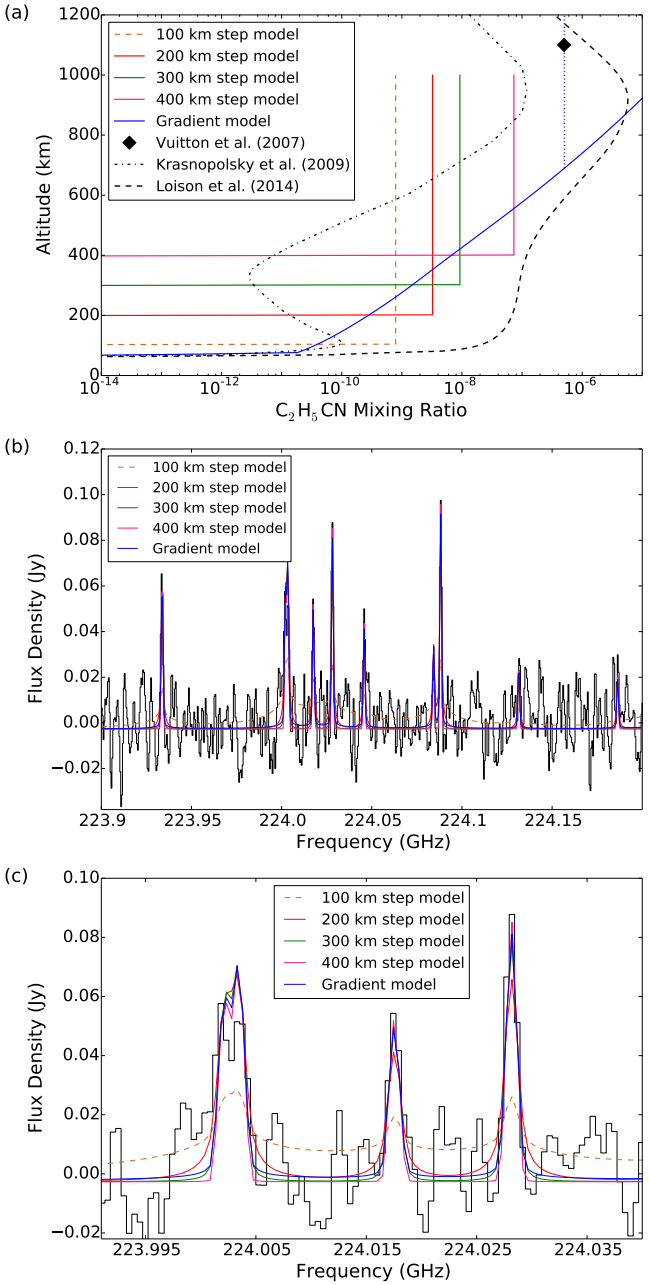

FIG. 3.— (a) VMR profiles for the best-fitting C_2H_5CN models (parameters given in Table 2). The (poorly-fitting) 100 km step model is shown, as well as the INMS measurement of Vuitton et al. (2007) and the theoretical profiles from Krasnopolsky (2009) and Loison et al. (2014). Vertical dotted portion of the blue 'gradient model' curve shows a plausible alternative profile above 700 km. (b) Spectral region used for our model fits, containing some of the strongest observed C_2H_5CN lines (black histogram). The best-fitting C_2H_5CN models from panel (a) are shown with colored curves. (c) Close-up of the region surrounding three of the strongest C_2H_5CN emission features.

dance gradient for C_2H_5CN and its concentration at altitudes $\gtrsim 200$ km are consistent with production in the upper atmosphere, combined with a relatively short chemical lifetime that prevents it from building up at lower altitudes through vertical mixing.

A plausible alternative to the best-fitting gradient profile above 700 km is indicated with a dotted vertical line in Fig. 3a, passing through the 5×10^{-7} abundance at $z = 1,100$ km, measured by Vuitton et al. (2007). The modeled C_2H_5CN column density above 700 km is small, so this alternative curve also provides an excellent fit to the observed spectrum. The altitude of peak sensitivity of our measurements depends on the assumed VMR profile shape, but for reasonable profiles that do not exceed the abundance measurement of Vuitton et al. (2007) at high altitude, the resulting spectra are most sensitive to C_2H_5CN at altitudes less than 600 km.

In Fig. 3a, we plot for comparison the C_2H_5CN VMR profiles predicted by the chemical models of Krasnopolsky (2009) and Loison et al. (2014). In the $z \approx$ 200-600 km region from which the majority of our observed emission originates, neither chemical model matches well with our retrieved VMR profiles. The Krasnopolsky (2009) model produces C_2H_5CN through the reaction of excited nitrogen atoms with C_3H_6, and the resulting stratospheric/mesospheric abundance is up to three orders of magnitude lower than implied by our observations. This indicates that a significant C_2H_5CN production channel is missing from the model. Conversely, C_2H_5CN abundances calculated by Loison et al. (2014) exceed those of our retrieved profiles by 1-3 orders of magnitude at altitudes 100-300 km, where our model is quite well constrained. In their model, C_2H_5CN is produced from the ternary association reaction of CH_2CN and CH_3 (+ M), which has not been measured in the laboratory. The apparent shortcomings of these models highlight a lack of knowledge regarding Titan's C_2H_5CN chemistry. Improved chemical models are currently in development (*e.g.* Vuitton et al. 2014).

The production of C_2H_5CN in the mid and upper atmosphere on Titan could plausibly be the result of gas-phase chemistry involving binary ion-molecule or neutral-neutral reactions. Production and subsequent release from the surfaces of solid (haze) particles or ices also cannot be ruled out — C_2H_5CN is abundant in the environments surrounding young stellar objects, where its formation is generally believed to result from reactions on the surfaces of dust grains (*e.g.* Bisschop et al. 2007; Bottinelli et al. 2007). As yet, there are no known neutral gas-phase routes to the formation of ethyl cyanide in low pressure astrophysical environments, and our results identify a clear need for further laboratory and theoretical studies in this regard. Recombination of $C_2H_5CNH^+$ is known to produce C_2H_5CN (Vigren et al. 2010), so ion-molecule synthesis of this nitrile ion should also be examined.

4.2. *Molecular Emission Maps*

Combining the derived vertical profile with the observed emission maps, the three-dimensional distribution of C_2H_5CN relative to other atmospheric species provides important clues regarding its origin. The observed molecular contour maps in Fig. 2 show evidence for significant north-south extension of each species. This extension is consistent with the presence of emission from near both poles, which is highlighted in the case of HC_3N, for which two closely-separated emission components (one over each pole) could plausibly give rise to the observed contour structure. Indeed, Cordiner et al. (2014) observed the HC_3N $J = 40-39$ transition towards Titan in November 2013 at slightly higher angular resolution, and identified two clear emission peaks for this molecule, one centered near each pole. Such polar enhancement(s) are characteristic of the abundance patterns seen by Voyager and Cassini in photochemical product species, theorized to result from the combined effects of Titan's atmospheric chemistry and circulation (Coustenis & Bézard 1995; Teanby et al. 2008; Coustenis et al. 2010; Vinatier et al. 2010; Teanby et al. 2012).

The C_2H_5CN emission map (Fig. 2a) shows a surprising spatial distribution, with a significant (7σ) flux enhancement

over the southern pole relative to the north. This is the opposite trend to that observed for the other three species, which show clear enhancements in the northern hemisphere. Differences in stratospheric temperature between Titan's northern and southern hemispheres have been found to be generally $\lesssim 15\%$ (Coustenis & Bézard 1995; Flasar et al. 2005; Achterberg 2008). Our observed emission lines are relatively invariant to such small temperature changes, so spatial variations in the gas temperature are an unlikely explanation for the observed asymmetries. Molecular abundance peaks near Titan's north pole have previously been identified for HC_3N and CH_3CCH (during northern winter), so it seems plausible that the emission structures observed with ALMA are due to intrinsic latitudinal abundance variations. As a caveat, the temperatures in Titan's polar mesosphere are known to vary on rapid timescales (*e.g.* Teanby et al. 2012; de Kok et al. 2014), and temperature information for the epoch of our observations is lacking, so further work will be needed to firmly establish the relative distributions of these species.

An explanation for the southerly C_2H_5CN peak is due to the transition of Titan's seasons from northern winter in 2002 to **(late)** northern spring in 2012. During this time, the reversal of Titan's main atmospheric circulation cell is expected to channel fresh photochemical products from mid latitudes towards the south pole (Teanby et al. 2012). Meanwhile, gases transported north during the previous season remain concentrated around the north pole, undergoing slow photochemical destruction. Following the northern winter, species with longer chemical lifetimes should remain in the north for longer while those with shorter lifetimes disappear, and reappear in the south. Our maps therefore suggest a shorter chemical lifetime for C_2H_5CN than for HC_3N, CH_3CN and CH_3CCH. This hypothesis can be tested by observing the evolution of the distributions of these species over the coming years, particularly during the transition from northern spring to the summer solstice in 2017.

5. SUMMARY

Nineteen separate emission features from 27 rotational transitions of C_2H_5CN were detected in Titan's atmosphere using ALMA archival spectra recorded in July 2012.

Radiative transfer modeling indicates that most of the observed C_2H_5CN is concentrated at altitudes > 200 km. This is consistent with production in the upper atmosphere, combined with a relatively short chemical lifetime that inhibits downward mixing. The observed C_2H_5CN emission maps suggest a higher abundance in the south polar region than the north (in contrast to HC_3N, CH_3CN, and CH_3CCH, which peak in the north), again consistent with a relatively short chemical lifetime for C_2H_5CN and south polar subsidence. This possibility can be verified through future measurements of temporal variations in the spatial distributions of the observed species with respect to Titan's changing seasons.

In order to help ascertain the origin of ethyl cyanide on Titan (and in other astrophysical environments), new laboratory studies of possible gas-phase routes to C_2H_5CN are required.

This research was supported by NASA's Planetary Atmospheres and Planetary Astronomy programs, The Goddard Center for Astrobiology, The Leverhulme Trust and the UK Science and Technology Facilities Council. It makes use of ALMA data set ADS/JAO.ALMA#2011.0.00319.S. ALMA is a partnership of ESO (representing its member states), NSF (USA) and NINS (Japan), together with NRC (Canada) and NSC and ASIAA (Taiwan), in cooperation with the Republic of Chile. The Joint ALMA Observatory is operated by ESO, AUI/NRAO and NAOJ. The National Radio Astronomy Observatory is a facility of the National Science Foundation operated under cooperative agreement by Associated Universities, Inc.

REFERENCES

Achterberg, R. K., Conrath, B. J., Gierasch, P. J., Flasar, F. M., Nixon, C. A. 2008, Icarus, 194, 263
Bézard, B., Yelle, R., & Nixon, C. A. 2014, in Titan: Surface, Atmosphere and Magnetosphere, Ed.s I. Muller-Wodarg, C. Griffith, E. Lellouch and T. Cravens, Chap. 6, Cambridge University Press, 158
Bisschop S. E., Jørgensen, J. K., van Dishoeck, E. F., de Wachter, E. B. M. 2007, A&A, 465, 913
Bottinelli, S., Ceccarelli, C., Williams, J. P., Lefloch, B. 2007, A&A, 463, 601
Boucher, D., Burie, J., Dubrulle, A., Demaison, J. 1980, J. Phys. Chem. Ref. Data, 9, 659
Brauer, C. S., Pearson, J. C., Drouin, B. J., Yu, S. 2009, ApJSS, 184, 133
Capone, L. A., Prasad, S. S., Huntress, W. T. et al. 1981, Nature, 293, 45
Coll, P., Coscia, D., Smith, N. et al. 1999, PSS, 47, 1331
Cordiner, M. A., Nixon, C. A., Teanby, N. A. et al. 2014, ApJL, 795, L30
Coustenis, A., Bézard, B. 1995, Icarus, 115, 126
Coustenis, A., Jennings, D. E. & Nixon, C. A. et al. 2010, Icarus, 207, 461
de Kok, R., Irwin, P. G. J., Teanby, N. A. 2008, Icarus, 197, 572
de Kok, R., Teanby, N. A., Maltagliati, L., Irwin, P. G. J., Vinatier, S. 2014, Nature, 514, 65
Dubrulle, A., Boucher, D., Burie, J. Demaison, J. 1978, J. Mol. Spect., 72, 158
Flasar, F. M., Achterberg, R. K. Conrath, B. J. et al. 2005, Science, 308, 975
Fulchignoni, M., Ferri, F., Angrilli, F. et al. 2005, Nature, 438, 785
Fujii, T., Arai, N., 1999, AJ, 519, 858
Irwin, P. G. J., Teanby, N. A., de Kok, R. et al. 2008, J. Quant. Spec. Radiat. Transf., 109, 1136
Khanna, R. K. 2005, Icarus, 177, 116
Krasnopolsky, V. A. 2009, Icarus, 201, 226
Lide, D., Kehiaian, H., 1994. CRC Handbook of Thermophysical and Thermochemical Data. CRC Press, Boca Raton, FL.
Loison, J. C., Hébrard E., Dobrijevic, M. et al. 2014, Icarus, in press
Marten, A., Hidayat, T., Biraud, Y., & Moreno, R. 2002, Icarus, 158, 532
McMullin, J. P., Waters, B., Schiebel, D., Young, W. & Golap, K. 2007, in Astronomical Society of the Pacific Conference Series, Vol. 376, Astronomical Data Analysis Software and Systems XVI, ed. R. A. Shaw, F. Hill, & D. J. Bell, 127
Moreno, R., Lellouch, E., Lara, L. M. et al. 2012, Icarus, 221, 753
Müller, H. S. P., Thorwirth, S., Roth, D. A., Winnewisser, G. 2001, A&A, 370, L49
Teanby, N. A., de Kok, R., Irwin, P. G. J. et al. 2008, Icarus, 193, 595
Teanby, N. A., Irwin, P. G. J., Nixon, C. A. et al. 2012, Nature, 491, 732
Teanby, N. A., Irwin, P. G. J., Nixon, C. A. et al. 2013, Planet. Space Sci., 75, 136
Thompson, W.R., Henry, T.J., Schwartz, J.M., Khare, B.N., Sagan, C. 1991, Icarus, 90, 57
Thorwirth, S., Müller, H. S. P. & Winnewisser, G. 2000, J. Mol. Spec., 204, 133
Vigren, E., Hamberg, M., Zhaunerchyk, V. et al. 2010, ApJ, 722, 847
Vinatier, S., Bézard, B., Nixon, C. A. et al. 2010, Icarus, 205, 559
Vuitton, V., Yelle, R. V. & McEwan, M. J. 2007, Icarus, 191, 722
Vuitton, V., Yelle, R. V., Klippenstein, S. J., Hörst, S. M.; Lavvas, P. 2014, American Astronomical Society, DPS meeting #46, #105.01
Wilson, E. H. & Atreya, S. K. 2004, J. Geophys. Res., 109, 6002